Silva, E.; Bastos, A.C.; Neto, M.; Fernandes, A.J.; Silva, R.; Guerreiro, M.; Ferreira, S.; Zheludkevich, M.; Oliveira, F.:

New fluorinated diamond microelectrodes for localized detection of dissolved oxygen

In: Sensors and Actuators B (2014) Elsevier

DOI: 10.1016/j.snb.2014.07.127

New Fluorinated Diamond Microelectrodes for Localized Detection of Dissolved Oxygen

E.L. Silva[1], A.C Bastos[1], M.A. Neto[1], A.J.S. Fernandes[2], R.F. Silva[1], M.G.S. Ferreira[1], M.L. Zheludkevich[1,3], F.J. Oliveira[1]

1 - CICECO – Department of Materials and Ceramics Engineering, University of Aveiro, 3810-193 Aveiro - Portugal
2 – Physics Department, University of Aveiro, 3810-193 Aveiro, Portugal
3 - MagIC, Institute of Materials Research, Helmholtz-Zentrum Geesthacht, Max-Planck Str. 1, 21502 Geesthacht, Germany

Abstract

The present work reports on a novel needle type oxygen microsensor based on boron doped diamond (BDD) with tailored surface aiming in better electrochemical performance. The microelectrodes are produced by growing diamond films using HFCVD (Hot Filament Chemical Vapor Deposition) on top of electrochemically sharpened tungsten filaments. The diamond is functionalized using CF_4 RF-plasma post-treatments resulting in fluorine termination of the surface.
The quantitative detection of the dissolved oxygen (DO) is demonstrated and supported with successful fitting to the theoretical values calculated for diffusion limited current on hemicylinder shape electrode. The developed MEs were calibrated and tested as probes for microamperometric mapping of dissolved oxygen in a Zn-Fe wire-electrode model galvanic couple immersed in 50 mM NaCl. Modified diamond MEs show a fast and stable response towards oxygen mapping, as well as stability for several days of measurements.

Keywords: Boron doped diamond; Microelectrodes; Dissolved oxygen; Surface modification

1. Introduction

Dissolved oxygen is one of the prime oxidizing species involved in cellular metabolism as well as in microbiological and corrosion processes [1,2]. In corroding systems, oxygen plays a major role in many cathodic reactions and is a key factor influencing the corrosion potential of a specific material in E-pH diagrams [3]. This influence is best demonstrated when a differential aeration corrosion cell is formed as it often happens in crevices and when biofilms are present. In more common corrosion forms like aqueous and atmospheric corrosion the reduction of DO is the main cathodic process occurring in neutral and alkaline media, being less important at low pH [3]. Access to spatially resolved information on corrosion distribution and mechanisms can be made by localized scanning probe techniques like SECM (Scanning Electrochemical Microscopy) [4], SVET (Scanning Vibrating Electrode Technique) [5], SRET (Scanning Reference Electrode Technique) [6], micropotentiometry [7], microamperometry [8], etc. The degree of spatial resolution that these techniques provide has motivated their use in various microscopic studies e.g. on galvanic corrosion [9], pitting corrosion [10], examination of defective coatings [11], and “smart” coatings [12], effect of inhibitor addition [13], etc. Clark-type electrodes are the most commonly used oxygen sensors and their function is based on an integrated three-electrode cell insulated in glass [14]. Oxygen permeates through a Teflon or polyethylene membrane at the extremity of the electrode and is reduced at the Pt disk after diffusing through a KCl electrolyte. Introduced in 1953, the reliability of Clark type electrodes for oxygen sensing has even inspired miniaturized versions, although not at a true microscale [15]. Platinum and gold have been demonstrated as suitable alternatives in the form of recessed disk microelectrodes [16,17]. However, the reduction of other species in the potential range of oxygen reduction, electrode fouling in biological environments or surface deactivation after longer measurement periods, in the case of platinum, may interfere with the measurement and impose frequent cleaning and calibration procedures [17].
Boron doped CVD (Chemical Vapor Deposition) polycrystalline diamond has been increasingly attracting the interest of electrochemists as material for electrodes thanks to its well documented electrochemical properties, which include wide electrochemical

potential window for water electrolysis, high-signal-to-noise ratio, high chemical stability and resistance to fouling [18,19]. Depending on the growth conditions, the microstructure of CVD diamond will present a variable sp^2/sp^3 carbon ratio, with the surface being normally hydrogen terminated under standard growth conditions.
Previous studies by Fujishima and co-workers indicate that the reduction of DO on boron doped diamond electrodes relies on the amount of sp^2 carbon [20,21]. This is consistent with our previous report where boron doped nanocrystalline diamond microelectrodes (MEs) were used for Zn^{2+} and DO sensing, although the DO measurements were merely qualitative, i.e., no calibration curve nor quantification were determined [22].
One of the advantages of CVD diamond is the possibility of functionalization with various heteroatoms such as O, F, Cl, and others, based on relatively easy procedures [23,24]. By doing so it is possible to adjust the properties of this material for targeting specific analytes.
Plasma fluorination of diamond surfaces has been reported to allow further expansion of the already wide potential window of diamond for water electrolysis, although reducing the standard rate constant, k_0, for certain redox couples like Eu^{3+}/Eu^{2+}, Fe^{3+}/Fe^{2+} and $Fe[CN]_6^{3-}/Fe[CN]_6^{4-}$ [25]. Other effects include the removal of sp^2 carbon by CF_4 plasma [26]. Moreover the possibility of DO complexation by fluorocarbon compounds has been demonstrated unveiling their possible applicability in the solid state [27].
This work reports the fabrication and application of novel oxygen sensitive boron doped diamond microelectrodes modified by CF_4 plasma (F-BDD). After calibration with an optical commercial oxygen sensor device, the plasma modified MEs were used for microamperometric mapping of DO oxygen close to the surface of galvanically coupled Zn and Fe model wire-electrodes immersed in a corrosive electrolyte.

2. Experimental

Boron doped diamond (BDD) microelectrodes were fabricated by coating electrochemically sharpened tungsten filaments with a thin layer of BDD by HFCVD

(Hot Filament CVD) techniques. A 91.7% H_2 + 4.6% CH_4 mixture was used for diamond film growth. The remaining 3.7% gas phase was provided by the doping source: a mixture of B_2O_3 dissolved in ethanol, dragged by Argon gas through a gas washing bottle containing the mixture and finally into the CVD chamber. Four tungsten filaments at 2300ºC provided activation of the gas species with a total chamber pressure of 50 mbar, while the substrate was kept at a constant temperature of 800º C. After a growth period of 30 minutes, the methane and boron flow were stopped and the samples were exposed only to activated hydrogen during 30 minutes before cooling down the reactor, to ensure that all the diamond coated tips where H-terminated.

Afterwards the MEs were submitted to a CF_4 RF-plasma (EMITECH K1050X, Quorum Tech., UK) treatment for 5 minutes. In order to evaluate the effect of each plasma on surface modification, planar tungsten substrates (1x1 cm) were coated with equal diamond films as the ones on the MEs, because of limitations inherent to the characterization equipment. Hence, the surface of the planar diamond films was characterized by XPS (X-ray Photoelectron Spectroscopy) (Kratos AXIS Ultra HAS, UK) using a monochromatic Al Kα X-ray source (1486.7 eV), before and after plasma modification. The binding energy of the C1s peak (285 eV) was used as reference and a charge correction of 0.9 eV was used for the unmodified sample.

The freshly assembled microelectrodes were calibrated by cyclic voltammetry (Ivium CompactStat potentiostat/galvanostat, Ivium, The Netherlands) with simultaneous comparison to response of an optical O_2 sensor (Hach HQ40d, US). A three electrode configuration with the BDD ME as working electrode, a Pt counter-electrode and an Ag/AgCl reference electrode was used for electrochemical measurements. Both an as-grown BDD and a fluorinated BDD MEs were immersed simultaneously and polarized in turns at a scan rate of 100 mV/s, by shifting the electrical connection. The concentration of dissolved oxygen in a 50 mM NaCl solution was controlled by Argon bubbling and a calibration curve was elaborated based on the diffusion limited current of oxygen reduction at the potential of -1.3 V.

A model system consisting of Zn-Fe galvanically coupled wire-electrode cell filled with 50 mM NaCl solution was used to evaluate the applicability of the microelectrodes for localized mapping of the O_2 concentration near active corroding metallic surfaces.

Microamperometry measurements were performed with an IPA2 amplifier (Applicable Electronics Inc., USA) in the voltammetric/amperometric mode, using a 2 electrode arrangement, with a Ag/AgCl electrode as counter and reference electrode. 2D X-Y scans were carried out using a microstepping motor driver (USDIGITAL, USA) at a distance of 100 µm between the diamond ME and the surface. X-Z scans permitted obtaining the normal distribution of species above the electrodes. Maps were recorded at -1.3 V (vs. Ag/AgCl) for detection of dissolved O_2.

3. Results and discussion

3.1 Microelectrode surface characterization

The B-doped diamond MEs exhibited a sub-micrometer roughness (100 nm – 1µm) which allows a good compromise between grain size and minimization of sp^2 impurities, i.e., a microstructure that accounts for sensor miniaturization and high crystalline quality. The diamond layers exhibit uniform coverage of the tungsten tips as shown by scanning electron microscopy observation (Fig. 1). After being submitted to the CF_4 plasma treatment, no observable microstructural changes were noticeable (Fig. 1a-b). This observation is in a good agreement with the results of other authors, after such a short treatment time [28]. The varnish insulation layer covered the full body of the diamond coated tungsten wire with exception of the apex, left uncovered to work as the electroactive surface with ~20 µm extension (Fig. 1c).

In order to evaluate the effect of plasma on surface termination, the surface of the equivalent planar films was analyzed by XPS before and after the treatments. Before plasma treatment a very small O 1s peak is distinguishable most likely because the boron source (B_2O_3+Et) already contains oxygen (Fig. 1d). After being exposed to the CF_4 plasma, the F1s peaks became much more prominent (Fig. 1e).

The available data concerning the components of the C1s spectra for diamond films gives an indication of how the growth and surface treating conditions can lead to significant shifts of the binding energies for each surface group, although they are

narrowed to typical ranges [29]. Thus, the C1s core level for both films was deconvoluted in order to tentatively identify the different bonding states of the surface carbon atoms. Before fluorination (Fig. 1f) the diamond surface exhibited high intensity bands at 285.0 and 285.4 eV, which were assigned to C-C (1) and C-H_x (2). Two other bands with lower intensity were identified at 284.6 and 287.4 eV, possibly corresponding to C=C (3) and C=O groups (4), respectively [29–31]. These four groups were identified after fluorination as well, (Fig. 1g) with a slight downshift in their binding energies. Four additional bands were identified, with probable correspondence to C-CF at 285.6 eV (5) [32], C-F at 286.6 eV (6), C-F_2 at 288.2 eV (7) and C-F_3 at 292.2 (8) [32-34].

3.2. Calibration of microelectrodes

The calibration procedure for the boron doped diamond MEs was performed at 21.7 º C and 987 mbar with simultaneous amperometric and optical measurement (Fig. 2a). As-grown and modified microelectrodes were immersed in NaCl 50 mM along with the reference electrode, an optical sensor and the tip of an Argon line. The oxygen concentration was decreased by stepwise Argon bubbling and voltammetry curves were recorded in turns with each electrode, after the optical sensor showed a stable oxygen concentration. Figs. 2b and 2c show the voltammetric curves of oxygen reduction on the non-treated BDD microelectrode and on the fluorinated one, respectively, with a plateau-like current response in the potential range from c.a. -1.2 to -1.6 V. Based on the current values obtained at -1.3 V, calibration curves for both MEs were determined (Fig. 3a-b). A poor linearity was observed for the non-treated ME with R^2=0.969 (Fig. 3a). In contrast, the F-BDD ME showed a strong linear correlation (R^2=0.9988) between points and a sensitivity of the electrode of 0.1422 ± 0.006 nA per µm of dissolved oxygen (Fig. 3b). The detection limit was determined to be 0.63 µM, which is in the same order of previous reports using platinum microdisks [17].

The calibration curve for the F-BDD microelectrode was also fitted according to the theoretical derivation for the diffusion limited quasi-steady state current observed at a hemicylinder (Fig. 3c and Eq. (1)) [35], where *n* is the number of transferred electrons, *F*

is the Faraday constant, *A* is the electrode area, *D* is the diffusion coefficient for oxygen (c.a. -2.20×10^{-5} cm^2 s^{-1} for pure water [36]), *C* is the analyte concentration, *r* is the electrode radius and *t* is the time of the forward voltammetric scan. Attempts were also made for the conical and prolate hemispheroidal shapes, but none of them fitted the experimental points in an adequate way.

$$i_{qss}^{cylinder} = \frac{2nFADC}{rln\left(\frac{4Dt}{r}\right)} \qquad (1)$$

3.3. Microamperometric mapping of dissolved oxygen

The obtained high correlation of the measurement results to the theoretical model confers applicability of the developed F-BDD microelectrode for quantitative detection of DO in aqueous electrolytes. However the microelectrode must also have a fast response time in order to be applicable for localized amperometric mapping.
A model galvanic wire-electrode cell was created for localized electrochemical tests of the newly developed MEs. The main aim of these experiments is to demonstrate the applicability of the developed electrodes for localized corrosion studies. The Zn-Fe electrochemical cell is schematically depicted in Figure 4a. In this system, a strong current decrease is expected at the iron cathode due to oxygen reduction at the surface of this metal. A less intense current reduction may also be observable at the anode, caused by the existence of local cathodic regions on zinc originated from additional self-corrosion of this metal, although the manifestation of this activity will depend on the surface condition and immersion time. The maps of oxygen concentration were obtained amperometrically by scanning a 5x2 mm area at 100 µm above the galvanic cell surface. The scans were done with 100 µm point-to-point distance, in a continuous back and forth mode starting from the upper left corner of the rectangular area depicted in Fig. 4b. The scan rate was adjusted according to waiting time between each ME position, and current averaging time.

The fluorinated diamond ME were polarized at -1.3 V allowing to map the distribution of dissolved O_2 (Fig. 5a), showing a strong depletion of this gas above the cathodic region, and minor depletion above the zinc anode. Several MEs were tested, evidencing their reproducibility. A long term stability during several days of measurement was also observed as can be seen from comparison of maps obtained with a fresh electrode and one after 4 days of use (Fig. 5b).

Furthermore a comparison was made relatively to as-grown MEs with low non diamond carbon content. The results are depicted in Fig. 6. The CF_4-treated ME demonstrate fast response for DO mapping, with much lower averaging and waiting times per point, down to 0.01 s for both, with negligible distortion and difference in current intensity (Fig. 6a-c). Increasing the scan rate in the case of the non-fluorinated microprobes caused an obvious patterning effect due to signal delay as a result of lower responsiveness (higher response time) towards oxygen reduction (Fig 6d-e). Although a detailed study was not performed, the complexity of the corroding media with the presence of zinc ions, corrosion products and variable pH suggests that the operation of F-BDD microelectrodes remains unperturbed in environments where multiple species at different concentrations coexist.

Diamond electrodes have been reported to be insensitive to DO, in both alkaline and acid media. Any oxygen associated response has been assigned to the presence of sp^2 carbon material, especially in acid media, while being considered highly unfavorable at sp^3 bonded carbon [20]. The metastable growth of CVD diamond, within the graphite domain of stability, implicates that sp^2 bonded carbon will always be present, even in high purity polycrystalline diamond, in residual amounts. Thus, sp^2 carbon is possibly the main factor associated to the response of the hydrogen-terminated diamond microelectrodes here presented, particularly considering the poor linearity observed.

In the case of surface modification with CF_4 plasma, there is evidence pointing in another direction. The Raman spectra of a fluorinated microelectrode is depicted in Fig. 7. An intense diamond peak at 1336 cm^{-1} is observable, along with a very weak contribution from trans-polyacetylene and from the D and G bands, confirming the high crystalline quality of the fluorinated diamond film. Moreover the complexation of DO by fluorinated hydrocarbons has been previously demonstrated. Buchachenko et al. [27]

have reported, by NMR measurements on polyfluoro organic compounds dissolved in ciclo hexane, that DO can be complexed in similar amounts by CF_2 and CF_3 groups, with negligible contribution from CH_2 and CH_3 groups, and also from double bonds. Hence, it is proposed that a similar effect may be observed in the solid state, at the fluorinated diamond surface, with the carbon-fluorine groups functioning as O_2 capturers. The formation of complexed O_2 at the F-BDD surface then creates favorable conditions for the molecule to be reduced by the ME. This mechanism is also favored by chemical stability of C-F bonds [37]. Although the current density tends to be lower by the action of surface fluorine groups, these offer a number of advantages. The wider range of water stability of fluorinated diamond ensures that oxygen reduction can occur without interference of hydrogen evolution [25], isolating the oxygen-due response; the intrinsically low background currents ensure higher detection limit, while the CF_4 plasma treatment *per se* reduces significantly the non-diamond carbon contributions, which are related to undesired adsorption effects, higher double-layer charging current and chemical instability [38].

Hence, upon undergoing fluorination treatment in CF_4 plasma, diamond surfaces were demonstrated to be responsive to DO. The fast response, low detection limit and long term stability exhibited by these sensors allows their application for localized measurements on corrosion systems where high oxygen concentration gradients are frequently observed, along with the presence of other ions and corrosion products. The possibility of gathering a localized oxygen distribution map in a few minutes is another important advantage. A future work will be presented reporting on the influence of specific ions on the response of the microelectrodes under operation in model corrosion systems.

4. Conclusions

The novel diamond based microelectrode for oxygen detection is reported. The fluorination of diamond-based microelectrodes by CF_4 plasma creates functional C-F

groups on the diamond surface that can lead to improvement of sensibility, limit of detection and response time for localized amperometric detection of DO in aqueous electrolyte solutions. Upon calibration with a commercial optical oxygen sensor it was possible to determine a sensitivity of the electrode of 0.1422 ± 0.006 nA with a detection limit of 0.63 µM. By microamperometric tests with a model galvanic cell it was shown that fluorinated diamond MEs can provide detection of oxygen distribution, exhibiting fast response and long term stability, especially when higher scanning rates are used. The comparison between H-terminated diamond microelectrodes and fluorinated ones confirms that in the first case the responsiveness to DO is most likely associated to sp^2 carbon, due to the poor linearity of the calibration curve and slow response. Conversely, upon plasma fluorination of the diamond surface, the reduction in sp^2 carbon content corresponded to a strong linearity of the calibration curve, faster response and low detection limit, which provides evidence that the surface fluorine groups may work as complexating agents for DO. Hence, the newly developed diamond-based microelectrodes can represent a reliable option for challenging localized electrochemical measurements where common electrode solutions are not suitable.

Acknowledgements

E.L. Silva, M.A. Neto would like to acknowledge FCT (Fundação para a Ciencia e a Tecnologia) for the grants SFRH/BD/61675/2009, and SFRH/BPD/45610/2008, respectively. This work was supported by projects PTDC/CTM/108446/2008, PTDC/CTM-MET/113645/2009, funded by FEDER through COMPETE programmme-Operacional Factors for Competitivity and by national funds through FCT – Portuguese Science and Technology Foundation. The FP7 Marie-Curie Programe is also gratefully acknowledged for the support proided in frame of SISET (FP7-PEOPLE-2010-IRSES Reference 269282) and PROAIR (FP7-PEOPLE-2013-IAPP Reference 612415) projects.

References

[1] S. Jouanneau, L. Recoules, M.J. Durand, A. Boukabache, V. Picot, Y. Primault, et al., Methods for assessing biochemical oxygen demand (BOD): A review., Water Res. 49C (2013) 62–82.

[2] R.M. Wightman, Probing Cellular Chemistry with in Biological Systems Microelectrodes, 311 (2012) 1570–1574.

[3] V. 13- Corrosion, ASM Handbook, 9th ed., 1987.

[4] A.J. Bard, F.R.F. Fan, D.T. Pierce, P.R. Unwin, D.O. Wipf, F.M. Zhou, Chemical Imaging of Surfaces with the Scanning Electrochemical Microscope, Science (80-.). 254 (1991) 68–74.

[5] H.S. Isaacs, The Use of the Scanning Vibrating Electrode Technique for Detecting Defects in Ion Vapor-Deposited Aluminum on Steel, Corrosion. 43 (1987) 594–598.

[6] P. Marcus, F. Mansfeld, Analytical Methods in Corrosion Science and Engineering, CRC Press, Florida, 2006.

[7] A.C. Bastos, M.G. Taryba, O.V. Karavai, M.L. Zheludkevich, S.V. Lamaka, M.G.S. Ferreira, Micropotentiometric mapping of local distributions of Zn2+ relevant to corrosion studies, Electrochem. Commun. 12 (2010) 394–397.

[8] A.C. Bastos, O. V. Karavai, M.L. Zheludkevich, K.A. Yasakau, M.G.S. Ferreira, Localised Measurements of pH and Dissolved Oxygen as Complements to SVET in the Investigation of Corrosion at Defects in Coated Aluminum Alloy, Electroanalysis. 22 (2010) 2009–2016.

[9] K.B. Deshpande, Experimental investigation of galvanic corrosion: Comparison between SVET and immersion techniques, Corros. Sci. 52 (2010) 2819–2826.

[10] H. Krawiec, V. Vignal, R. Oltra, Use of the electrochemical microcell technique and the SVET for monitoring pitting corrosion at MnS inclusions, Electrochem. Commun. 6 (2004) 655–660.

[11] M.C. Yan, V.J. Gelling, B.R. Hinderliter, D. Battocchi, D.E. Tallman, G.P. Bierwagen, SVET method for characterizing anti-corrosion performance of metal-rich coatings, Corros. Sci. 52 (2010) 2636–2642.

[12] Y. González-García, J.M.. Mol, T. Muselle, I. De Graeve, G. Van Assche, G. Scheltjens, et al., SECM study of defect repair in self-healing polymer coatings on metals, Electrochem. Commun. 13 (2011) 169–173.

[13] K. Mansikkamaki, U. Haapanen, C. Johans, K. Kontturi, M. Valden, Adsorption of benzotriazole on the surface of copper alloys studied by SECM and XPS, J. Electrochem. Soc. 153 (2006) B311–B318.

[14] Z.T. L.C. Clark Jr., R. Wolf, D. Granger, Continuous recording of blood oxygen tensions by polarography, J. Appl. Physiol. 8 (1953) 189–193.

[15] J. Park, J. Chang, M. Choi, J.J. Pak, D.-Y. Lee, Y.K. Pak, Microfabirated Clark-type Sensor for Measuing Dissolved Oxygen, 2007 IEEE Sensors. (2007) 1412–1415.

[16] T.-S. Lim, J.-H. Lee, I. Papautsky, Effect of recess dimensions on performance of the needle-type dissolved oxygen microelectrode sensor, Sensors Actuators B Chem. 141 (2009) 50–57.

[17] M. Sosna, G. Denuault, R.W. Pascal, R.D. Prien, M. Mowlem, Development of a reliable microelectrode dissolved oxygen sensor, Sensors Actuators B Chem. 123 (2007) 344–351.

[18] A.F. Azevedo, M.R. Baldan, N.G. Ferreira, Nanodiamond Films for Applications in Electrochemical Systems, Int. J. Electrochem. 2012 (2012) 1–16.

[19] A. Fujishima, T.N. Rao, B. V Sarada, Electroanalytical applications of bare and modified diamond electrodes, Diam. Mater. Vii, Proc. 2002 (2001) 127–138.

[20] T. Yano, E. Popa, D.A. Tryk, K. Hashimoto, A. Fujishima, Electrochemical behavior of highly conductive boron-doped diamond electrodes for oxygen reduction in acid solution, J. Electrochem. Soc. 146 (1999) 1081–1087.

[21] T. Yano, D.A. Tryk, K. Hashimoto, A. Fujishima, Electrochemical behavior of highly conductive boron-doped diamond electrodes for oxygen reduction in alkaline solution, J. Electrochem. Soc. 145 (1998) 1870–1876.

[22] E.L. Silva, A.C. Bastos, M.A. Neto, R.F. Silva, M.L. Zheludkevich, M.G.S. Ferreira, et al., Boron doped nanocrystalline diamond microelectrodes for the detection of Zn2+ and dissolved O-2, Electrochim. Acta. 76 (2012) 487–494.

[23] T. Kondo, H. Ito, K. Kusakabe, K. Ohkawa, Y. Einaga, A. Fujishima, et al., Plasma etching treatment for surface modification of boron-doped diamond electrodes, Electrochim. Acta. 52 (2007) 3841–3848.

[24] A. Hartl, E. Schmich, J.A. Garrido, J. Hernando, S.C.R. Catharino, S. Walter, et al., Protein-modified nanocrystalline diamond thin films for biosensor applications, Nat Mater. 3 (2004) 736–742.

[25] S. Ferro, A. De Battisti, Physicochemical properties of fluorinated diamond electrodes, J. Phys. Chem. B. 107 (2003) 7567–7573.

[26] H.B. Martin, A. Argoitia, J.C. Angus, U. Landau, Voltammetry studies of single-crystal and polycrystalline diamond electrodes, J. Electrochem. Soc. 146 (1999) 2959–2964.

[27] A.L. Buchachenko, M.Y. Pokrovskaya, Complexation of Molecular Oxygen with Organic Fluorine-Containing Molecules, Bull. Acad. Sci. USSR, Div. Chem. Sci. 33 (1985) 2451.

[28] T. Kondo, H. Ito, K. Kusakabe, K. Ohkawa, K. Honda, Y. Einaga, et al., Characterization and electrochemical properties of CF4 plasma-treated boron-doped diamond surfaces, Diam. Relat. Mater. 17 (2008) 48–54.

[29] S. Ferro, M. Dal Colle, A. De Battisti, Chemical surface characterization of electrochemically and thermally oxidized boron-doped diamond film electrodes, Carbon 43 (2005) 1191-1203.

[30] X.C. LeQuan, W.P. Kang, J.L. Davidson, B.K. Choi, Y.M. Wong, R. Barbosa, et al., Effect of rearranging sp(2)/sp(3) hybridized-bonding on the field emission characteristics of nano-crystalline diamond films, Diam. Relat. Mater. 18 (2009) 200–205.

[31] A. Denisenko, A. Romanyuk, C. Pietzka, J. Scharpf, E. Kohn, Surface damages in diamond by Ar/O-2 plasma and their effect on the electrical and electrochemical characteristics of boron-doped layers, J. Appl. Phys. 108 (2010) 074901-074901-7.

[32] A. Denisenko, A. Romanyuk, C. Pietzka, J. Scharpf, E. Kohn, Electronic surface barrier properties of fluorine-terminated boron-doped diamond in electrolytes, Surf. Sci. 605 (2011) 632–637.

[33] A. Denisenko, A. Romanyuk, C. Pietzka, J. Scharpf, E. Kohn, Surface structure and surface barrier characteristics of boron-doped diamond in electrolytes after CF_4 plasma treatment in RF-barrel reactor, Diam. Relat. Mater. 19 (2010) 423–427.

[34] K. Kanda, N. Yamada, K. Yokota, M. Tagawa, M. Niibe, M. Okada, et al., Fabrication of fluorine-terminated diamond-like carbon thin film using a hyperthermal atomic fluorine beam, Diam. Relat. Mater. 20 (2011) 703–706.

[35] R.M. Wightman, Chronopotentiometric current at hemicylinder and band microelectrodes: theory and experiment, J. Electroanal. Chem. 217 (1987) 417–423.

[36] I.C. Wang, Simultaneous measurement of oxygen diffusion coefficients and solubilities in electrolyte solutions with a polarographic oxygen electrode, Chem. Eng. Sci. 43 (1988) 3093–3107.

[37] A.K. Tiwari, J.P. Goss, P.R. Briddon, N.G. Wright, A.B. Horsfall, R. Jones, et al., Thermodynamic stability and electronic properties of F- and Cl-terminated diamond, Phys. Status Solidi a-Applications Mater. Sci. 209 (2012) 1709–1714.

[38] A. Argoitia, H.B. Martin, J.C. Angus, U. Landau, Single-crystal, polycrystalline, and chemically modified diamond electrodes: A voltammetric comparison, Proc. Fifth Int. Symp. Diam. Mater. 97 (1998) 364–376.

Figure 1

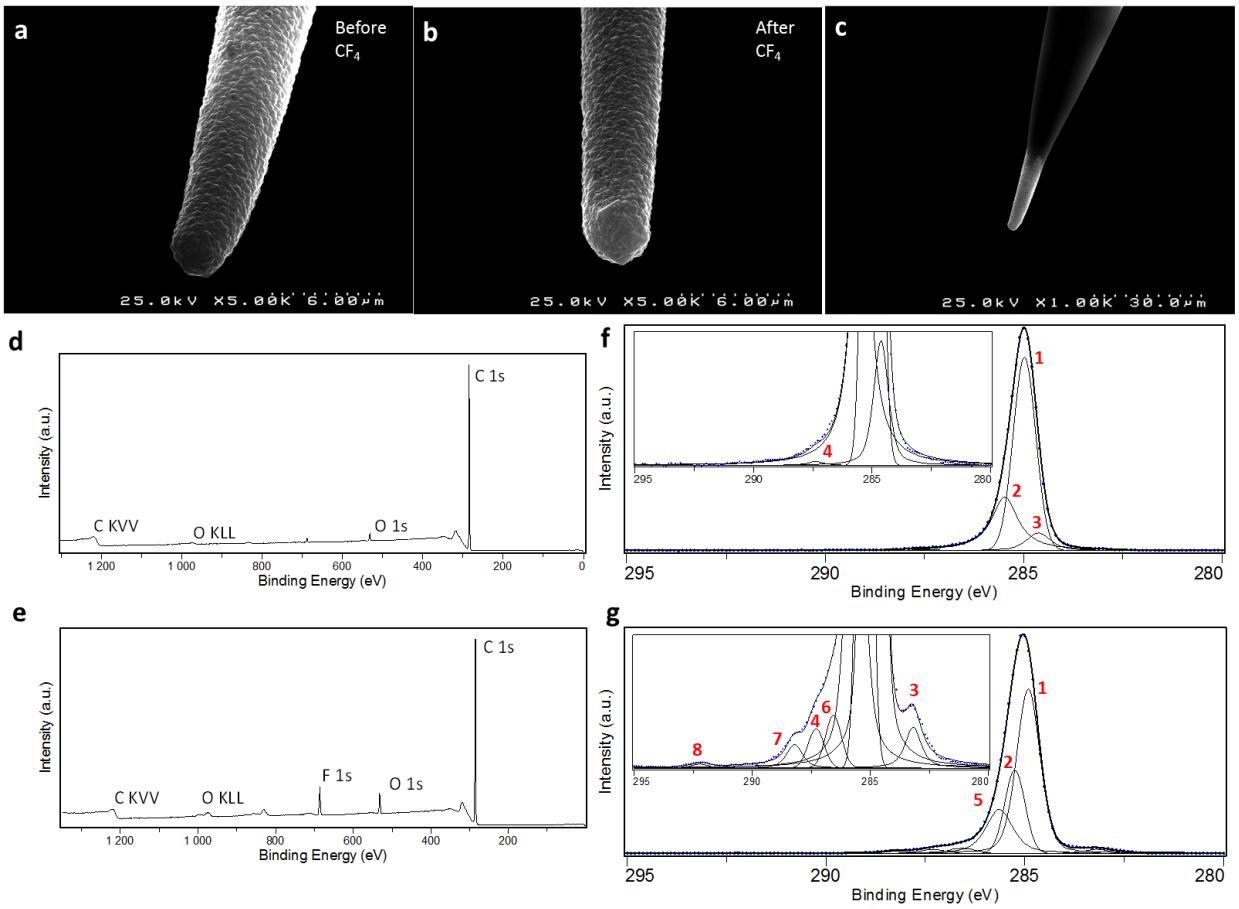

Fig. 1 – Boron doped diamond microelectrode for which the surface condition a) before and b) after plasma treatment are shown. The insulated microelectrode is shown in c). The XPS spectra for identification of the surface groups on the diamond films is presented for d, f) as-grown diamond and e, g) fluorinated diamond.

Figure 2

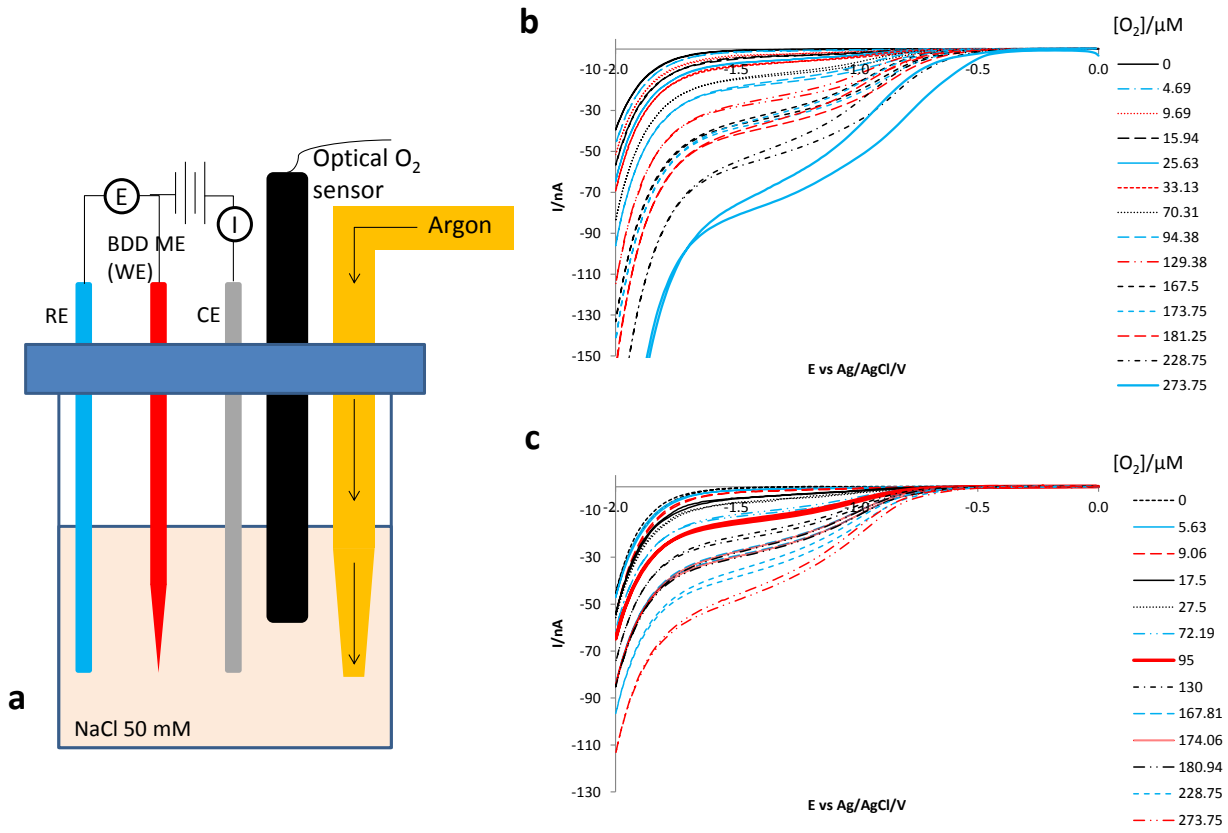

Fig. 2 – Voltammetry for diamond microelectrode calibration. a) Experimental setup for dissolved oxygen calibration with the measurements were taken in NaCl 50mM for normal oxygen saturation and for successively lower concentrations established by Argon bubbling through the solution; b) and c) Polarization curves taken at 100 mV/s with different oxygen concentrations from 0 to 273.75 µM, at 21.7 ºC and 1001 mbar for an as-grown and a F-BDD microelectrode, respectively.

Figure 3

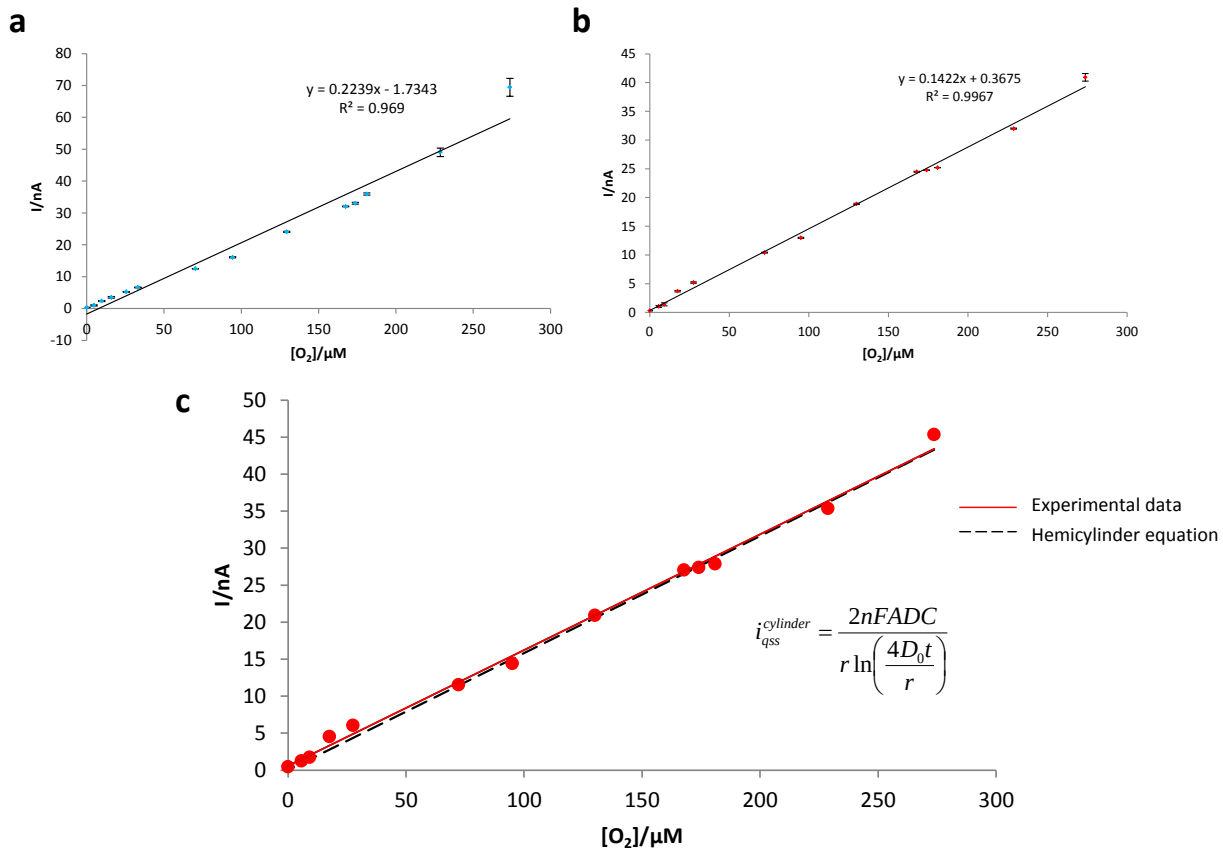

Fig. 3 - Calibration curves for both electrode types showing a) weak linearity for the as-grown BDD ME (R^2=0.969) and b) stronger correlation between points through the whole concentration range for the F-BDD ME (R^2=0.9967). In c) the calibration curve of the F-BDD ME is reasonably matched by equating the quasi-steady state current of a hemicylinder microelectrode geometry.

Figure 4

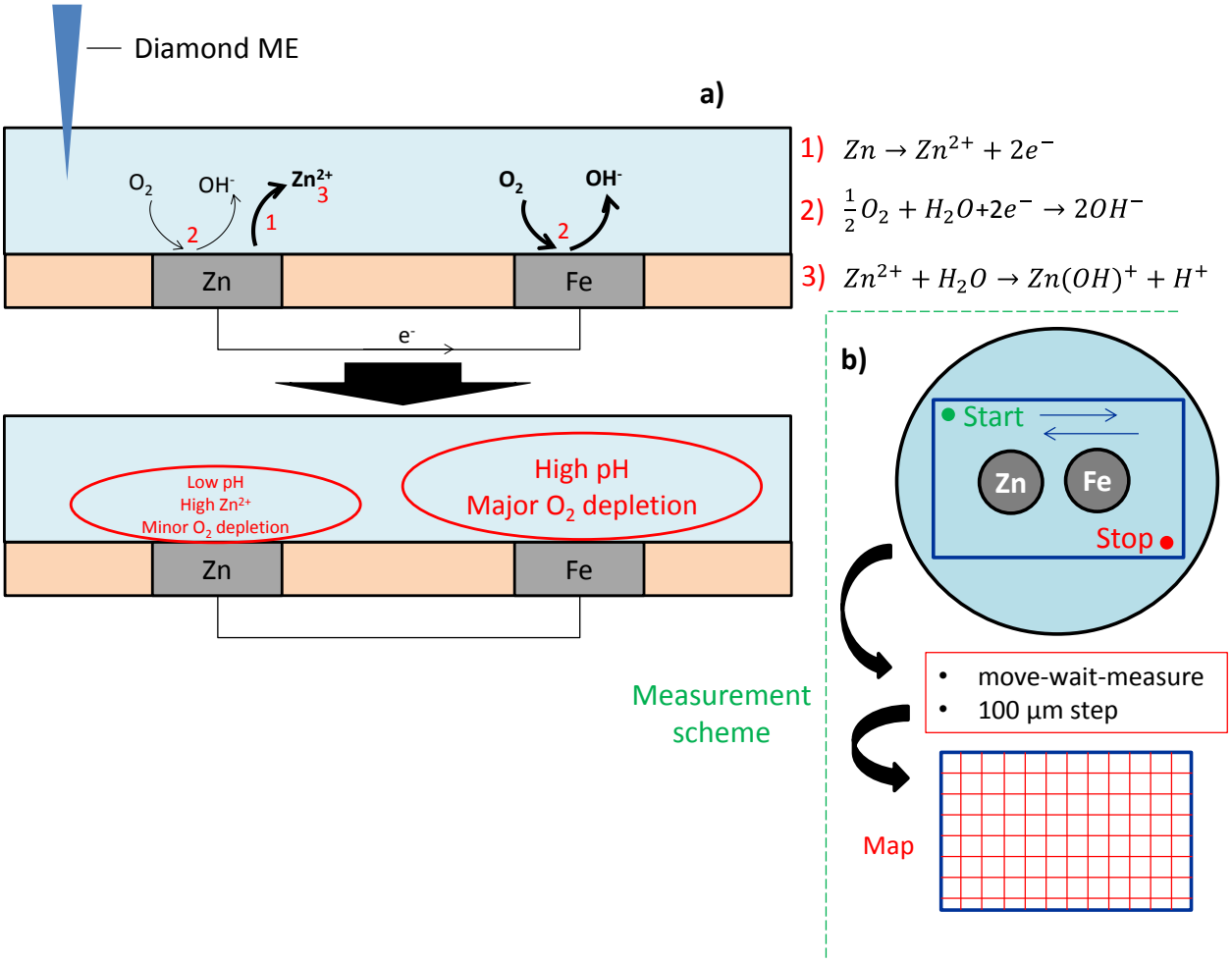

Fig. 4 - Experimental setup for the microamperometric measurements. (a) Zn-Fe galvanic couple immersed in 50 mM NaCl for dissolved oxygen detection, with indication of the reactions associated to galvanic corrosion (b) Schematics of the measurements performed.

Figure 5

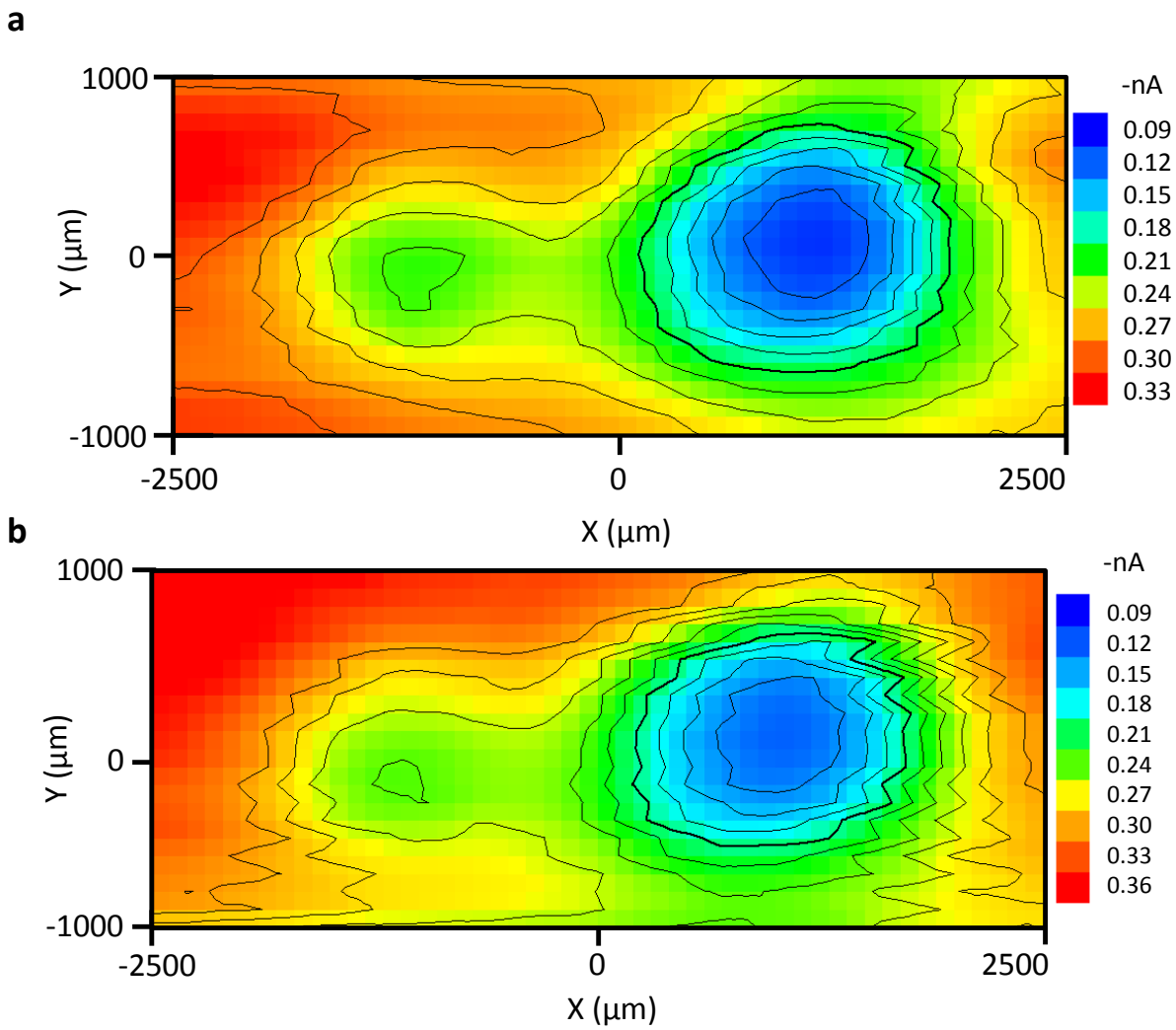

Fig. 5 - Dissolved oxygen distribution map recorded at -1.3 V with a) a fresh diamond ME modified by CF_4 plasma; b) after 4 days of measurement.

Figure 6

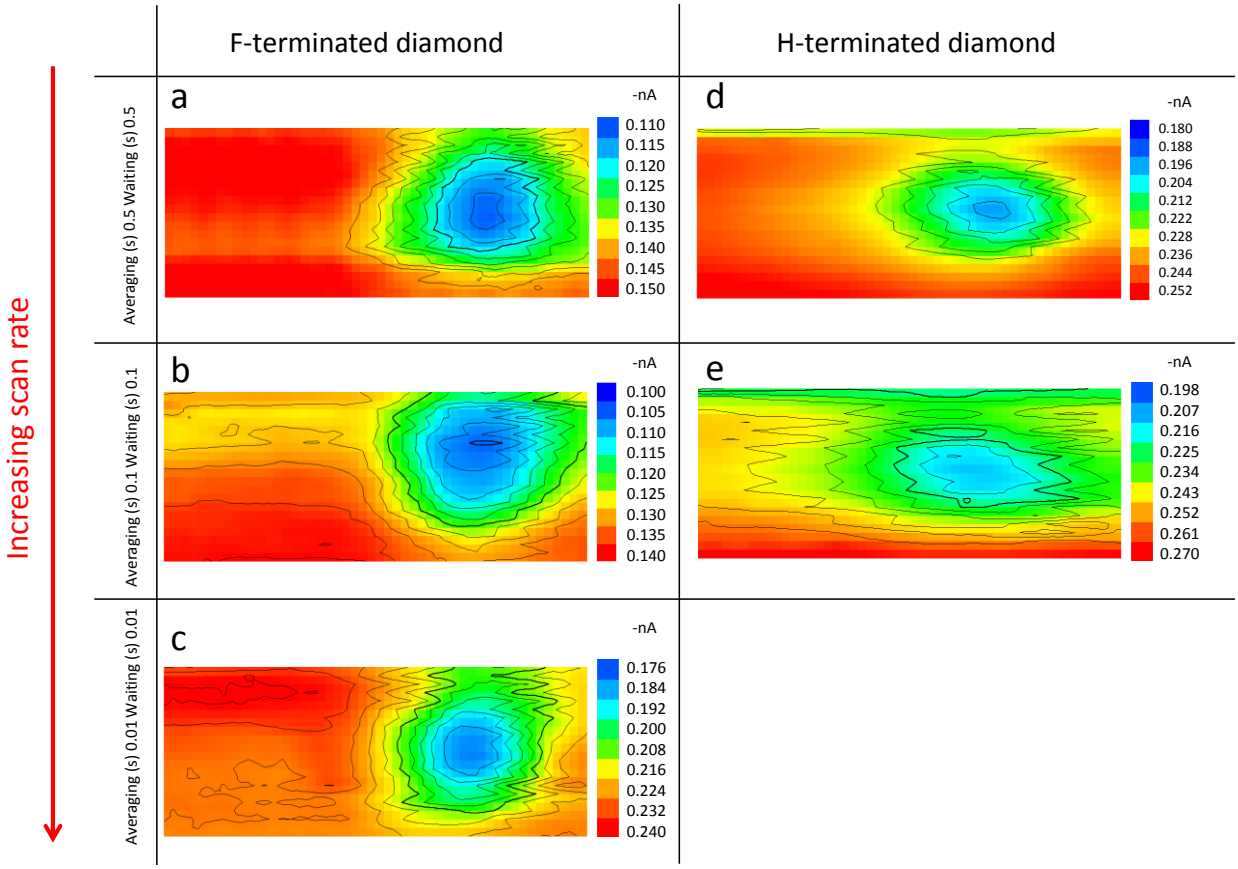

Fig. 6 - Dissolved oxygen concentration maps recorded with a diamond ME treated with CF_4 plasma and an as-grown ME, polarized at -1.3 and -0.9 V, respectively, with varying averaging-waiting times.

Figure 7

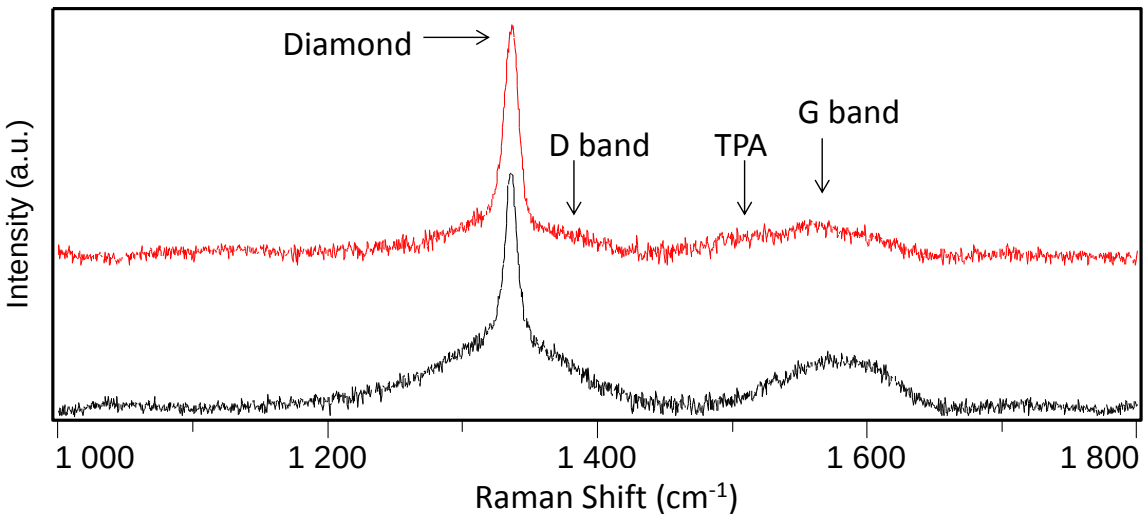

Fig. 7 – Raman spectra of as-grown (black line) and F-BDD (red line) MEs, showing a negligible sp^2 carbon content in the latter case.